Prediction of pseudogap formation due to d-wave bond-order in organic superconductor κ-(BEDT-TTF)$_2$X

Rina Tazai,[1] Youichi Yamakawa,[1] Masahisa Tsuchiizu,[2] and Hiroshi Kontani [1]

[1]*Department of Physics, Nagoya University, Furo-cho, Nagoya 464-8602, Japan*
[2]*Department of Physics, Nara Women's University, Nara 630-8506, Japan*

Rich hidden unconventional orders with pseudogap formation, such as the intersite bond order (BO), attract increasing attention in condensed matter physics. Here, we investigate the hidden order formation in organic unconventional superconductor κ-(BEDT-TTF)$_2$X. We predict the formation of d-wave BO at wavelength $\boldsymbol{q} = \boldsymbol{Q}_{\mathrm{B}} = (\delta, \delta)$ $(\delta = 0.38\pi)$ for the first time, based on both the functional renormalization group (fRG) and the density-wave equation theories. The origin of the BO is the quantum interference among antiferromagnetic spin fluctuations. This prediction leads to distinct pseudogap-like reduction in the NMR $1/T_1$ relaxation rate and in the density-of-states, consistently with essential experimental reports. The present theory would be applicable for other strongly correlated metals with pseudogap formation.

The layered organic compounds κ-(BEDT-TTF)$_2$X attract considerable attention because of their rich variety of ground states due to strong electron correlation. Many compounds show the antiferromagnetic (AFM) insulating states at ambient pressure [1,2], except for several quantum spin-liquid compounds [like X = Cu$_2$(CN)$_3$] [3]. Under pressure, many of them show unconventional superconductivity ($T_c \gtrsim 10$ K) next to the AFM phase [1,2]. In X=Cu[N(CN)$_2$]Br and X=Cu(NCS)$_2$, metallicity and superconductivity appear even at ambient pressure. Up to now, $d_{x^2-y^2}$ and/or d_{xy} symmetries are predicted based on the spin-fluctuation mechanisms [4–8], the VMC study [9], and cluster DMFT study [10].

A central mystery in anomalous metallic states in κ-(BEDT-TTF)$_2$X would be the origin of the pseudogap and its relation to the superconductivity. Both the NMR relaxation ratio $1/T_1T$ [1,2] and the density-of-states (DOS) measured by the STM [11] exhibit gap behaviors below $T^* \sim 50$ K. As origins of the pseudogap, for example, crossover scenarios due to strong spin or superconducting (SC) fluctuations [12–20] and proximity effect to Mottness [21,22] have been discussed. However, distinct kink-like changes observed in $1/T_1T$ [1,2] and in the hardening of optical phonon frequency [23] indicates the emergence of a hidden order parameter at $T \approx T^*$. (The intradimer charge disproportionation is reported only in X = Cu$_2$(CN)$_3$ [9].)

The similarity between κ-(BEDT-TTF)$_2$X and cuprate high-T_c superconductors has been actively discussed for years. Recently, in many cuprates, the charge density-wave (DW)

order in period $3a \sim 4a$ at $T_{\mathrm{CDW}} \sim 200$ K has been discovered by the x-ray scattering, STM study, and NMR analysis [24–29]. In addition, nematic transition (presumably at $\boldsymbol{q} = \boldsymbol{0}$) emerges at the pseudogap temperature T^* ($> T_{\mathrm{CDW}}$) [30–34]. These charge-channel phase transitions at T_{CDW} and T^* have been hotly discussed based on the charge/spin current order [35–37], and d-wave bond-order (BO) scenarios [38–48]. The BO is the modulation of correlated hopping integrals, and it can be caused by the paramagnon interference mechanism [45–48] that is overlooked in usual spin-fluctuation theories. This mechanism has also been applied to Fe-based superconductors [49–53] and heavy-fermion systems [54]. Thus, it is significant to study the paramagnon interference effects in κ-(BEDT-TTF)$_2$X to go beyond the conventional understanding of this system.

In this paper, we discuss the occurrence of hidden charge DW orders in κ-(BEDT-TTF)$_2$X by using both the functional renormalization group (fRG) and the DW equation methods. We predict the d-wave BO order formation at wavelength $\boldsymbol{q} = \boldsymbol{Q}_{\mathrm{B}} = (\delta, \delta)$ $(\delta = 0.38\pi)$ in κ-(BEDT-TTF)$_2$X for the first time. The origin of the BO is novel quantum interference among paramagnons with $\boldsymbol{Q}_{\mathrm{S}}^{\pm} \approx (\pi \pm \delta/2, \pi \pm \delta/2)$. The predicted distinct reductions in the spin-fluctuation strength and in the DOS at BO transition temperature naturally explain the NMR and Raman measurements.

To analyze the quantum interference in low-dimensional metals, the fRG method is very powerful and reliable, since various DW instabilities (both particle-particle and particle-hole channels) are treated on the same footing [41,46,47,55–59]. Using the fRG, unconventional DW states in cuprates and ruthenates have been analyzed satisfactorily [47,58]. The fRG method is suitable to analyze the many-body electronic states, and we can obtain reliable results by making careful comparison with the diagrammatic calculation using the DW equation method [47,51–53].

FIG. 1. (a) Anisotropic triangular lattice for κ-(BEDT-TTF)$_2$X. (b) Band dispersion and (c) the FS at $n = 1$. The major nesting vector is $\boldsymbol{Q}_S \approx (\pi - \delta/2, \pi - \delta/2)$ and the minor nesting vector is $\boldsymbol{Q}_B \approx (\delta, \delta)$ with $\delta \approx 3\pi/8$. (d) Differential equation of the fRG theory. The crossed line represents electron propagator inside of the energy cutoff ($|\epsilon_{k'}| < \Lambda_l$), while the slashed line denotes on-shell one ($|\epsilon_k| = \Lambda_l$).

Here, we introduce the anisotropic triangular lattice dimer Hubbard model, which is the simplest effective model for κ-(BEDT-TTF)$_2$X; $\hat{H} = \hat{H}_0 + \hat{H}_U$ [60]. The kinetic term is given by $\hat{H}_0 = \sum_{k\sigma} \epsilon_k c_{k\sigma}^\dagger c_{k\sigma}$ with $\epsilon_k = 2t(\cos k_x + \cos k_y) + 2t' \cos(k_x + k_y)$. Indices $\boldsymbol{k}$ and σ denote the momentum and spin, respectively. Here, we set the hopping integrals in Fig. 1(a) as $(t, t') = (-1, -0.5)$. We verified that similar numerical results are obtained for $t'/t = 0.5 \sim 0.8$, which is realized in many compounds [61]. The on-site Coulomb interaction term is given by $\hat{H}_U = \sum_{k_1,k_2,k_3,k_4} \frac{1}{4} \Gamma^0_{k_1,k_2,k_3,k_4} c_{k_1}^\dagger c_{k_2} c_{k_3} c_{k_4}^\dagger \cdot \delta_{k_1-k_2-k_3+k_4,\mathbf{0}}$, where $k_i = (\boldsymbol{k}_i, \sigma_i)$ and $\mathbf{0}$ is the zero vector in the reduced zone. The initial four-point vertex is $\Gamma^0_{k_1,k_2,k_3,k_4} = U(\delta_{\sigma_1,\sigma_3}\delta_{\sigma_2,\sigma_4} - \delta_{\sigma_1,\sigma_2}\delta_{\sigma_3,\sigma_4})$. The four-point vertex acquires the momentum dependence after the renormalization, which is uniquely divided into the spin and charge parts as $\Gamma^0_{k_1,k_2,k_3,k_4} = \frac{1}{2}\Gamma^{0c}_{k_1,k_2,k_3,k_4}\delta_{\sigma_1,\sigma_2}\delta_{\sigma_4,\sigma_3} + \frac{1}{2}\Gamma^{0s}_{k_1,k_2,k_3,k_4}(\vec{\sigma})_{\sigma_1,\sigma_2} \cdot (\vec{\sigma})_{\sigma_4,\sigma_3}$. The initial condition $\Gamma^{0s} = -\Gamma^{0c} (= U)$ is largely modified by the renormalization.

In the following numerical study, we set the energy unit $|t| = 1$, and put the temperature $T = 0.05$ and the electron filling $n = 1$ ($\mu = 0.55$). The band structure and the Fermi surface (FS) are presented in Figs. 1(b) and 1(c), respectively. The patch indices ($1 \sim 64$) are shown on the ellipsoid electron pockets. The total band width is $W_D \sim 10$ (in unit $|t| = 1$), and

$|t|$ corresponds to 0.05 eV since $W_D \sim 0.5$ eV experimentally [5,60].

In the present study, we analyze the model by applying the RG+cRPA method developed in Refs. [46,47,58,59], which is an efficient hybrid method between the fRG and the random-phase-approximation (RPA). Here, we introduce the higher-energy cutoff Λ_0 ($= 2$) and the logarithmic energy mesh $\Lambda_l = \Lambda_0 e^{-l}$ with $l \geqslant 0$. Then, the effective four-point vertex $\hat{\Gamma}$ is derived from the one-loop RG equation in Fig. 1(d), by including the on-shell contribution $\Lambda_{l+dl} < |\epsilon_k - \mu| \leqslant \Lambda_l$ step-by-step. In strongly correlated systems, $\hat{\Gamma}$ strongly deviates from $\hat{\Gamma}^0$. In this procedure, the Brillouin zone (BZ) is divided into N_p patches; see the Supplemental Materials (SM) A [62]. Below, we set $\Lambda_0 = 2$ and $N_p = 64$. (Numerical results are not sensitive to the choices of Λ_0 and N_p.) We analyze the higher energy region $|\epsilon_k - \mu| \geqslant \Lambda_0$, where the vertex corrections (VCs) are less important, based on the constrained RPA (cRPA) with high numerical accuracy using fine $\boldsymbol{k}$ meshes. By using the RG+cRPA method, we can perform reliable calculations [46,47,58].

In Fig. 1(d), the 1st and 2nd terms on right-hand side represent the particle-hole (ph) scattering channels, and the 3rd term represents the particle-particle (pp) scattering channel. The RG flow starts from $l = 0$ ($\Lambda_l = \Lambda_0$) to $l \to \infty$ ($\Lambda_l \to 0$). In the parallel way, we solve the RG equation for the susceptibilities [58]. The RG flow will stop for $\Lambda_l \lesssim \omega_c$ with $\omega_c = \max\{T, \gamma\}$, where γ ($\propto |\mathrm{Im}\Sigma|$) is the quasiparticle damping rate. Considering large γ in κ-(BEDT-TTF)$_2$X, we introduce the low-energy cutoff $\omega_c = \pi T$ in the RG equation of the four-point vertex Γ in calculating Fig. 2 by following Refs. [46,47].

Here, we show numerical results for the dimer Hubbard model. First, we calculate various DW susceptibilities at $\omega = 0$ using the RG+cRPA method. The spin (charge) susceptibility with the form factor $f_x(\boldsymbol{k})$ is [47]

$$\chi^{s(c)}_x(\boldsymbol{q}) = \int_0^\beta d\tau \, \frac{1}{2}\langle A^{s(c)}_x(\boldsymbol{q}, \tau) A^{s(c)}_x(-\boldsymbol{q}, 0)\rangle, \qquad (1)$$

where $A^{s(c)}_x(\boldsymbol{q}) \equiv \sum_k f_x(\boldsymbol{k})(c^\dagger_{\boldsymbol{k}-\boldsymbol{q}/2\uparrow}c_{\boldsymbol{k}+\boldsymbol{q}/2\uparrow} - (+)c^\dagger_{\boldsymbol{k}-\boldsymbol{q}/2\downarrow} c_{\boldsymbol{k}+\boldsymbol{q}/2\downarrow})$. We calculate the spin and charge susceptibilities with the following form factors $f_1 = 1$, $f_x = \sqrt{2}\sin k_x$, $f_y = \sqrt{2}\sin k_y$, $f_{x^2-y^2} = \cos k_x - \cos k_y$, and $f_{xy} = 2\sin k_x \sin k_y$. As a result, we find that the spin susceptibility $\chi^S(\boldsymbol{q}) \equiv \chi^s_1(\boldsymbol{q})$ and the $d_{x^2-y^2}$-wave BO susceptibility $\chi^{BO}(\boldsymbol{q}) \equiv \chi^c_{x^2-y^2}(\boldsymbol{q})$ strongly develop. Other susceptibilities remain small in the present study.

In Figs. 2(a) and 2(b), we plot $\boldsymbol{q}$ dependencies of $\chi^S(\boldsymbol{q})$ and $\chi^{BO}(\boldsymbol{q})$ at $U = 3.5$. Strong spin fluctuations develop at $\boldsymbol{q} = \boldsymbol{Q}_S$, consistently with the previous RPA and FLEX analyses [5]. Moreover, we reveal the development of $\chi^{BO}(\boldsymbol{q})$ at $\boldsymbol{q} = \boldsymbol{Q}_B \approx (3\pi/8, 3\pi/8)$ in addition to $\boldsymbol{q} = (0, 0)$. The obtained strong bond fluctuations originate from the VCs that are dropped in the RPA.

The $\chi^{BO}(\boldsymbol{q})$ strongly develops by increasing U. Figure 2(c) shows the RG flow of the susceptibilities in the case of $U = 3.54$. In this case, the bond susceptibility exceeds the spin one after completing the renormalization. We see that $\chi^S(\boldsymbol{Q}_S)$ starts to increase in the early stage of the renormalization, by reflecting the major nesting of the FS at $\boldsymbol{q} = \boldsymbol{Q}_S$.
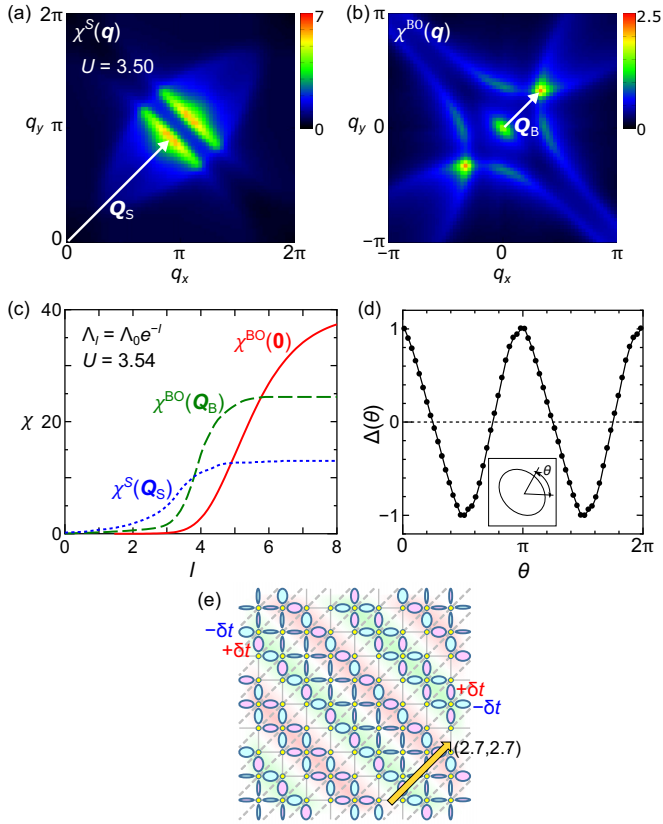
FIG. 2. The q dependencies of (a) $\chi^S(q)$ and (b) $\chi^{BO}(q)$ obtained by the RG+cRPA method at $U = 3.5$. (c) The RG flow for spin and BO susceptibilities at $U = 3.54$. (d) Obtained optimized SC gap function, which belongs to $d_{x^2-y^2}$-wave symmetry. (e) Schematic BO pattern at $q = Q_B$ in the real space, where $\lambda \approx (8/3, 8/3)$ is the wave vector.

Next, $\chi^{BO}(Q_B)$ starts to increase for $l \gtrsim 3$, and it exceeds $\chi^S(Q_S)$ at $l \sim 4$. Finally, $\chi^{BO}(0)$ starts to increase for $l \gtrsim 4$ ($\Lambda_l \lesssim 0.037$), because the renormalization of the Pauli ($q = 0$) susceptibility occurs only for $\Lambda_l \lesssim T$. All susceptibilities saturate for $l \gtrsim 8$ ($\Lambda_l \lesssim 0.7 \times 10^{-3}$). The final results in Figs. 2(a) and 2(b) are given at $l \approx 9$. Thus, all $\chi^S(Q_S)$, $\chi^{BO}(Q_B)$, and $\chi^{BO}(0)$ strongly develop at $U = 3.54$.

We also calculate the spin-singlet SC susceptibility [47],

$$\chi^{SC} = \frac{1}{2} \int_0^\beta d\tau \langle B^\dagger(\tau) B(0) \rangle, \quad \left(B \equiv \sum_k \Delta(k) c_{k\uparrow} c_{-k\downarrow} \right), \quad (2)$$

where $\Delta(k)$ is an even parity gap function, which is uniquely determined so as to maximize χ^{SC} under the constraint $\frac{1}{N} \sum_k |\Delta(k)|^2 \delta(\epsilon_k - \mu) = 1$ [47]. We show the obtained optimized gap at $U = 3.54$ in Fig. 2(d). The obtained gap function in the $d_{x^2-y^2}$-wave symmetry is understood as the spin-fluctuation-mediated d-wave state [5]. In the present case, large BO susceptibilities $\chi^{BO}(Q_B)$ and $\chi^{BO}(0)$ should contribute to the pairing mechanism [see Fig. 3(b)].

Figure 2(e) shows the schematic d-wave BO pattern at $q = Q_B$. Here, each red (blue) ellipse represents the increment (decrement) of the hopping integral δt_μ ($\mu = x, y$) caused by the BO parameters. The opposite sign between the adjacent δt_x and δt_y reflects the d-wave symmetry of the BO. The BO
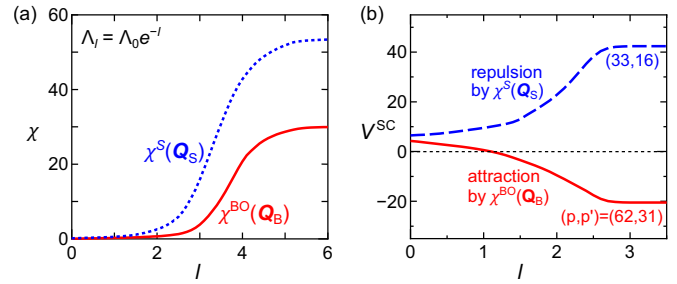
FIG. 3. Obtained RG results in the case of $\omega_c^{pp} = 10T$ at $U = 3.82$. (a) Obtained RG flow for $\chi^{BO}(Q_B)$ and $\chi^S(Q_S)$. (b) Obtained pairing interaction $V^{SC}(p, p')$ due to the spin-fluctuation-mediated repulsion [for $(p, p') = (33, 16)$] and the BO fluctuation-mediated attraction [for $(p, p') = (62, 31)$]. The patch number p and p' are shown in Fig. 1(c).

parameter causes the pseudogap in the DOS [see Figs. 4(d) and 4(e)].

Now, we clarify the importance of the spin fluctuations on the BO fluctuations. For this purpose, we solve the RG equation by dropping the contribution from the pp channel in the RG equation for Γ, by introducing an additional cutoff energy only for the pp channel; $\omega_c^{pp} (> \omega_c)$. Here, we set $\omega_c^{pp} = 10T$ to suppress the SC fluctuations selectively. The obtained
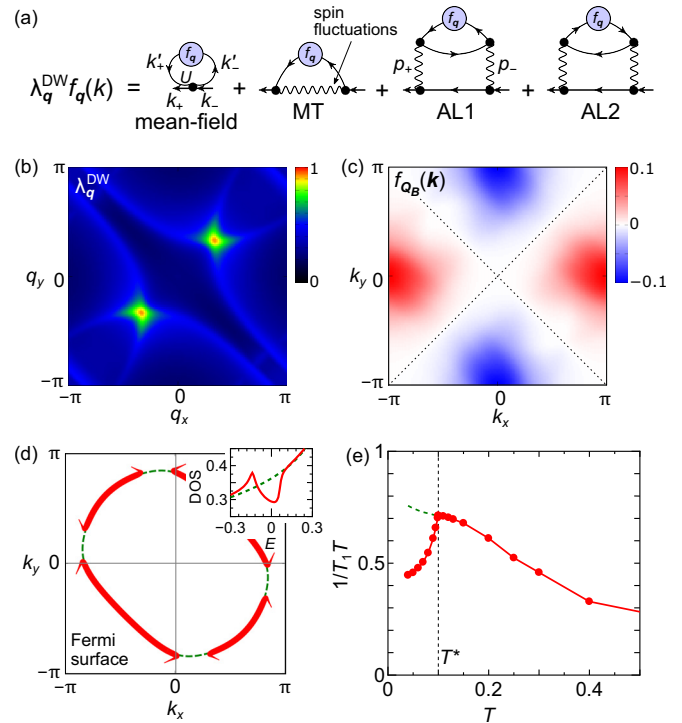
FIG. 4. (a) The DW equation for wave vector q. $k_\pm \equiv k \pm q/2$ and $p_\pm \equiv p \pm q/2$. The kernel function is composed of the mean field, MT, and AL terms 1 and 2. These diagrams are also produced systematically by solving the RG equation. (b) Obtained eigenvalue of the BO λ_q^{DW} and (c) the form factor $f_q(k)$ at $q = Q_B$ and $\epsilon_n = \pi T$. (d) Obtained Fermi arc structure in the unfolded zone, and the pseudogap in the DOS with $f^{max} = 0.1$ is shown in the inset. (e) Obtained $1/T_1 T$, where T^* is the BO transition temperature.

RG flows of the susceptibilities at $U = 3.82$ are shown in Fig. 3(a). We see that $\chi^S(\boldsymbol{Q}_S)$ starts to increase in the early stage, due to the ph channels in the RG equations in Fig. 1(d). Next, $\chi^{BO}(\boldsymbol{Q}_B)$ also increases to follow the increment of $\chi^S(\boldsymbol{Q}_S)$, similarly to Fig. 2(c). This result strongly indicates that the BO fluctuations are driven by the spin fluctuations. Note that $\chi^{BO}(\boldsymbol{Q}_B)$ exceeds $\chi^S(\boldsymbol{Q}_S)$ by setting $U = 3.86$ even in the case $\omega_c^{pp} = 10T$.

Next, we discuss the SC pairing vertex function $V^{SC}(\boldsymbol{p}, \boldsymbol{p}') = \frac{3}{2}\Gamma^s(\boldsymbol{p}, \boldsymbol{p}', -\boldsymbol{p}', -\boldsymbol{p}) - \frac{1}{2}\Gamma^c(\boldsymbol{p}, \boldsymbol{p}', -\boldsymbol{p}', -\boldsymbol{p}) - \Gamma^{0s}$ given by the RG+cRPA method [59]. Due to large ω_c^{pp} ($= 10T$), the obtained $V^{SC}(\boldsymbol{p}, \boldsymbol{p}')$ becomes "irreducible with respect to the pp channel" below ω_c^{pp}. Then, $V^{SC}(\boldsymbol{p}, \boldsymbol{p}')$ gives the "pairing interaction in the SC gap equation" with the BCS cutoff energy $\omega_{BCS} = \omega_c^{pp}$. The obtained RG flow of $V^{SC}(\boldsymbol{p}, \boldsymbol{p}')$ is shown in Fig. 3(b). The large repulsion for $\boldsymbol{p} - \boldsymbol{p}' \approx \boldsymbol{Q}_S$ is apparently given by the spin fluctuations. Interestingly, we find that the attraction for $\boldsymbol{p} - \boldsymbol{p}' \approx \boldsymbol{Q}_B$ is caused by the BO fluctuations in Fig. 3(a). The present result indicates that both $\chi^{BO}(\boldsymbol{Q}_B)$ and $\chi^S(\boldsymbol{Q}_S)$ cooperatively work as the pairing glue of the $d_{x^2-y^2}$-wave state, as understood in Fig. 1(c). The obtained gap structure is very similar to Fig. 2(d). Therefore, the d-wave BO fluctuations in the single-orbital Hubbard model can mediate large attractive pairing interaction.

Next, we explain that the BO fluctuations originate from the quantum interference between paramagnons, which is described by the Aslamazov-Larkin (AL) quantum process. For this purpose, we analyze the following DW equation [48,51–53]:

$$\lambda_{\boldsymbol{q}}^{DW} f_{\boldsymbol{q}}(k) = -\frac{T}{N}\sum_{k'} I_{\boldsymbol{q}}^c(k, k') G(k'_-) G(k'_+) f_{\boldsymbol{q}}(k'), \quad (3)$$

where $\lambda_{\boldsymbol{q}}^{DW}$ is the eigenvalue that represents the charge channel DW instability at wave vector $\boldsymbol{q}$. Here, $\boldsymbol{p}_\pm \equiv \boldsymbol{p} \pm \boldsymbol{q}/2$, and $k \equiv (\boldsymbol{k}, \epsilon_n)$ and $p \equiv (\boldsymbol{p}, \epsilon_m)$ (ϵ_n, ϵ_m are fermion Matsubara frequencies). The eigenfunction $f_{\boldsymbol{q}}(k)$ gives the form factor. The corresponding DW susceptibility is $\chi^{BO} \propto (1 - \lambda_{\boldsymbol{q}}^{DW})^{-1}$. In the present model, the obtained DW state corresponds to the d-wave BO.

The kernel function I^c is given by the Ward identity $-\delta\Sigma/\delta G$, which is composed of one single-paramagnon exchange term and two double-paramagnon exchange ones: The former and the latter are called the Maki-Thompson (MT) term and the AL terms, respectively; see Fig. 4(a). [Each wavy line is proportional to $\chi^S(\boldsymbol{q})$.] Among four terms in $I_{\boldsymbol{q}}^c$, the AL terms are significant for $\alpha_S \lesssim 1$, and they give spin-fluctuation-driven nematic orders in cuprates and Fe-based superconductors [48,49].

Figure 4(b) shows the obtained eigenvalue of the BO, $\lambda_{\boldsymbol{q}}^{DW}$, at $T = 0.05$ and $U = 2.53$, where the Stoner factor $\alpha_S = U\chi^0(\boldsymbol{Q}_S)$ is 0.90. Here, $\chi^0(\boldsymbol{q})$ is the irreducible susceptibility, and the SDW occurs when $\alpha_S = 1$. The eigenvalue $\lambda_{\boldsymbol{q}}^{DW}$ reaches almost unity at $\boldsymbol{q} = \boldsymbol{Q}_B$, which is consistent with $\chi^{BO}(\boldsymbol{q})$ given by the RG+cRPA in Fig. 2(b). The corresponding form factor in Fig. 4(c) possesses the $d_{x^2-y^2}$-wave symmetry. Therefore, strong $d_{x^2-y^2}$-wave BO susceptibility at $\boldsymbol{q} = \boldsymbol{Q}_B$ by the RG+cRPA method in Fig. 2(b) is well reproduced by the DW equation. The origin of the strong

BO instability at $\boldsymbol{q} = \boldsymbol{Q}_B$ is the AL terms in Fig. 4(a) that represent the quantum interference among paramagnons at $\boldsymbol{Q}_S^\pm \approx (\pi, \pi) \pm \boldsymbol{Q}_B/2$. [Note that $\chi^S(\boldsymbol{q})$ given by the RPA is similar to that the fRG result in Fig. 2(a).]

The paramagnon-interference mechanism can generate both the ferro-BO instability (at $\boldsymbol{q} = \boldsymbol{Q}_S^+ - \boldsymbol{Q}_S^\pm = 0$) and the incommensurate-BO one (at $\boldsymbol{q} = \boldsymbol{Q}_S^+ - \boldsymbol{Q}_S^- = \boldsymbol{Q}_B$). This mechanism causes the ferro-BO states in both Fe-based and cuprate superconductors according to the DW equation analysis [48,51–53]. In the present dimer Hubbard model, in contrast, the ferro-BO fluctuations remain small in the DW equation analysis. This is also true in the fRG analysis with $\omega_c^{pp} = 10T$ shown in Fig. 3. These results indicate that the paramagnon interference mechanism alone is not sufficient to establish large $\chi^{BO}(0)$ in Fig. 2(b). Therefore, we conclude that large $\chi^{BO}(0)$ is caused by the spin and SC fluctuations cooperatively, since the AL processes by SC fluctuations can cause the ferro-BO fluctuations according to Ref. [58].

Finally, we discuss the band folding and hybridization gap due to the BO with $\boldsymbol{q} = \boldsymbol{Q}_B$. Figure 4(d) shows the Fermi arc structure obtained for $f^{max} \equiv \max_k\{f_{\boldsymbol{Q}_B}(\boldsymbol{k})\} = 0.1$. Here, the folded band structure under the BO at $\boldsymbol{q} = \boldsymbol{Q}_B$ is "unfolded" into the original Brillouin zone [63] to make a comparison with ARPES experiment. The resultant pseudogap in the DOS is shown in the inset of Fig. 4(d), which is consistent with the STM study [11]. The BO leads to significant reduction of the spin-fluctuation strength, so the obtained $1/T_1 T \propto \sum_{\boldsymbol{q},\alpha,\beta} \mathrm{Im}\chi_{\alpha,\beta}^s(\boldsymbol{q}, \omega)/\omega|_{\omega=0}$ shown in Fig. 4(e) exhibit kink-like pseudogap behavior. Here, α, β represent the sites in the unit cell under the presence of the BO, and we set $f^{max} = 0.2 \times \tanh(1.74\sqrt{(1 - T/T^*)})$ below the BO transition temperature $T^* = 0.1$. [Here, $2f^{max}(T = 0)/T^* = 4$.] The obtained pseudogap behaviors in $1/T_1T$ and DOS are consistent with phase-transition-like experimental behaviors [1,2,23].

In the fRG study, the parquet VCs are generated by considering all ph, ph′, and pp channels in Fig. 1(d). On the other hand, in the DW equation study, the VCs are limited to MT and AL terms, whereas their frequency dependencies are calculated correctly. Both theoretical methods lead to the emergence of the *same d-wave bond-order* shown in Fig. 2(e).

In summary, we predicted the emergence of the d-wave BO at wave vector $\boldsymbol{q} = \boldsymbol{Q}_B = (0.38\pi, 0.38\pi)$ in κ-(BEDT-TTF)$_2$X, due to the interference between paramagnons with $\boldsymbol{Q}_S^\pm \approx (\pi, \pi) \pm \boldsymbol{Q}_B/2$. The BO is derived from both fRG method and the DW equation method. The BO transition leads to distinct pseudogap behaviors in the NMR $1/T_1$ relaxation rate and in the DOS, consistently with many experimental reports at $T \approx T^*$. As we show in the SM B [62], very similar numerical results are obtained in the case of $t'/t = 0.7$. Thus, the d-wave BO will be ubiquitous in κ-(BEDT-TTF)$_2$X. The present theory would be applicable for other strongly correlated metals with pseudogap formation.

[1] K. Kanoda, Electron correlation, metal-insulator transition and superconductivity in quasi-2D organic systems, (ET)$_2$X, Physica C **282-287**, 299 (1997).

[2] K. Kanoda and R. Kato, Mott physics in organic conductors with triangular lattices, Annu. Rev. Condens. Matter Phys. **2**, 167 (2011).

[3] Y. Shimizu, K. Miyagawa, K. Kanoda, M. Maesato, and G. Saito, Spin Liquid State in an Organic Mott Insulator with a Triangular Lattice, Phys. Rev. Lett. **91**, 107001 (2003).

[4] J. Schmalian, Pairing due to Spin Fluctuations in Layered Organic Superconductors, Phys. Rev. Lett. **81**, 4232 (1998).

[5] H. Kino and H. Kontani, Phase diagram of superconductivity on the anisotropic triangular lattice Hubbard model: An effective model of κ-(BEDT-TTF) salts, J. Phys. Soc. Jpn. **67**, 3691 (1998).

[6] H. Kondo and T. Moriya, Spin fluctuation-induced superconductivity in organic compounds, J. Phys. Soc. Jpn. **67**, 3695 (1998).

[7] H. Kontani and H. Kino, Theory of the Hall coefficient and resistivity for the layered organic superconductors κ-(BEDT-TTF)$_2$X, Phys. Rev. B **63**, 134524 (2001).

[8] K. Kuroki, Pairing symmetry competition in organic superconductors, J. Phys. Soc. Jpn. **75**, 051013 (2006).

[9] H. Watanabe, H. Seo, and S. Yunoki, Mechanism of superconductivity and electron-hole doping asymmetry in κ-type molecular conductors, Nat. Commun. **10**, 3167 (2019).

[10] B. Kyung and A.-M. S. Tremblay, Mott Transition, Antiferromagnetism, and d-Wave Superconductivity in Two-Dimensional Organic Conductors, Phys. Rev. Lett. **97**, 046402 (2006).

[11] T. Arai, K. Ichimura, K. Nomura, S. Takasaki, J. Yamada, S. Nakatsuji, and H. Anzai, Superconducting and normal-state gaps in κ-(BEDT-TTF)$_2$Cu(NCS)$_2$ studied by STM spectroscopy, Solid State Commun. **116**, 679 (2000).

[12] T. Kobayashi, Y. Ihara, Y. Saito, and A. Kawamoto, Microscopic observation of superconducting fluctuations in κ-(BEDT-TTF)$_2$Cu[N(CN)$_2$]Br by ^{13}C NMR spectroscopy, Phys. Rev. B **89**, 165141 (2014).

[13] Y. Eto, M. Itaya, and A. Kawamoto, Non-Fermi-liquid behavior of the organic superconductor κ-(BEDT-TTF)$_4$Hg$_{2.89}$Br$_8$ probed by ^{13}C NMR, Phys. Rev. B **81**, 212503 (2010).

[14] S. Tsuchiya, K. Nakagawa, J. Yamada, H. Taniguchi, and Y. Toda, Photoinduced phase separation with local structural ordering in organic molecular conductors, Phys. Rev. B **96**, 134311 (2017).

[15] K. Nakagawa, S. Tsuchiya, J. Yamada, and Y. Toda, Fluctuating superconductivity in κ-type organic compounds probed by polarized time-resolved spectroscopy, Europhys. Lett. **122**, 67003 (2018).

[16] H. Kontani, Anomalous transport phenomena in Fermi liquids with strong magnetic fluctuations, Rep. Prog. Phys. **71**, 026501 (2008).

[17] Y. Yanase T. Jujo, T. Nomura, H. Ikeda, T. Hotta, and K. Yamada, Theory of superconductivity in strongly correlated electron systems, Phys. Rep. **387**, 1 (2003).

[18] T. Moriya and K. Ueda, Spin fluctuations and high temperature superconductivity, Adv. Phys. **49**, 555 (2000).

[19] J. Schmalian, D. Pines, and B. Stojkovic, Weak Pseudogap Behavior in the Underdoped Cuprate Superconductors, Phys. Rev. Lett. **80**, 3839 (1998)

[20] B. Kyung, V. Hankevych, A. M. Dare, and A. M. S. Tremblay, Pseudogap and Spin Fluctuations in the Normal State of the Electron-Doped Cuprates, Phys. Rev. Lett. **93**, 147004 (2004).

[21] F. Kagawa, K. Miyagawa, and K. Kanoda, Unconventional critical behaviour in a quasi-two-dimensional organic conductor, Nature (London) **436**, 534 (2005).

[22] J. Kang, S.-L. Yu, T. Xiang, and J.-X. Li, Pseudogap and Fermi arc in κ-type organic superconductors, Phys. Rev. B **84**, 064520 (2011).

[23] M. Revelli Beaumont, P. Hemme, Y. Gallais, A. Sacuto, K. Jacob, L. Valade, D. de Caro, C. Faulmann, and M. Cazayous, Possible observation of the signature of the bad metal phase and its crossover to a Fermi liquid in κ-(BEDT-TTF)$_2$Cu(NCS)$_2$ bulk and nanoparticles by Raman scattering, J. Phys.: Condens. Matter **33**, 125403 (2021).

[24] G. Ghiringhelli, M. L. Tacon, M. Minola, S. Blanco-Canosa, C. Mazzoli, N. B. Brookes, G. M. D. Luca, A. Frano, D. G. Hawthorn, F. He, T. Loew, M. M. Sala, D. C. Peets, M. Salluzzo, E. Schierle, R. Sutarto, G. A. Sawatzky, E. Weschke, B. Keimer, and L. Braicovich, Long-range incommensurate charge fluctuations in (Y, Nd)Ba$_2$Cu$_3$O$_{6+x}$, Science **337**, 821 (2012).

[25] R. Comin, A. Frano, M. M. Yee, Y. Yoshida, H. Eisaki, E. Schierle, E. Weschke, . Sutarto, F. He, A. Soumyanarayanan, Y. He, M. L. Tacon, I. S. Elfimov, J. E. Hffman, G. A. Sawatzky, B. Keimer, and A. Damascelli, Charge order driven by Fermi-arc instability in Bi$_2$Sr$_{2-x}$La$_x$CuO$_{+\delta}$, Science **343**, 390 (2014).

[26] Y. Kohsaka, T. Hanaguri, M. Azuma, M. Takano, J. C. Davis, and H. Takagi, Visualization of the emergence of the pseudogap state and the evolution to superconductivity in a lightly hole-doped Mott insulator, Nat. Phys. **8**, 534 (2012).

[27] K. Fujita, M. H. Hamidian, S. D. Edkins, C. K. Kim, Y. Kohsaka, M. Azuma, M. Takano, H. Takagi, H. Eisaki, S. Uchida, A. Allais, M. J. Lawler, E.-A. Kim, S. Sachdev, and J. C. S. Davis, Direct phase-sensitive identification of a d-form factor density wave in underdoped cuprates, Proc. Natl. Acad. Sci. U.S.A. **111**, E3026 (2014).

[28] T. Wu, H. Mayaffre, S. Krämer, M. Horvatić, C. Berthier, P. L. Kuhns, A. P. Reyes, R. Liang, W. N. Hardy, D. A. Bonn, and M.-H. Julien, Emergence of charge order from the vortex state of a high-temperature superconductor, Nat. Commun. **4**, 2113 (2013).

[29] T. Wu, H. Mayaffre, S. Krämer, M. Horvatić, C. Berthier, W. N. Hardy, R. Liang, D. A. Bonn, and M.-H. Julien, Incipient charge order observed by NMR in the normal state of YBa$_2$Cu$_3$O$_y$, Nat. Commun. **6**, 6438 (2015).

[30] Y. Sato, S. Kasahara, H. Murayama, Y. Kasahara, E.-G. Moon, T. Nishizaki, T. Loew, J. Porras, B. Keimer, T. Shibauchi, and Y. Matsuda, Thermodynamic evidence for a nematic phase transition at the onset of the pseudogap in YBa$_2$Cu$_3$O$_y$, Nat. Phys. **13**, 1074 (2017).

[31] H. Murayama, Y. Sato, R. Kurihara, S. Kasahara, Y. Mizukami, Y. Kasahara, H. Uchiyama, A. Yamamoto, E.-G. Moon, J. Cai, J. Freyermuth, M. Greven, T. Shibauchi, and Y. Matsuda, Diagonal nematicity in the pseudogap phase of HgBa$_2$CuO$_{4+\delta}$, Nat. Commun. **10**, 3282 (2019).

[32] S. Nakata, M. Horio, K. Koshiishi, K. Hagiwara, C. Lin, M. Suzuki, S. Ideta, K. Tanaka, D. Song, Y. Yoshida, H. Eisaki, and A. Fujimori, Nematicity in the pseudogap state of cuprate superconductors revealed by angle-resolved photoemission spectroscopy, arXiv:1811.10028.

[33] K. Ishida, S. Hosoi, Y. Teramoto, T. Usui, Y. Mizukami, K. Itaka, Y. Matsuda, T. Watanabe, and T. Shibauchi, Divergent nematic susceptibility near the pseudogap critical point in a cuprate superconductor, J. Phys. Soc. Jpn. **89**, 064707 (2020).

[34] W. Wang, J. Luo, C. G. Wang, J. Yang, Y. Kodama, R. Zhou, and G.-Q. Zheng, Microscopic evidence for the intra-unit-cell electronic nematicity inside the pseudogap phase in $YBa_2Cu_4O_8$, Sci. China Phys. Mech. Astron. **64**, 237413 (2021).

[35] C. M. Varma, Non-Fermi-liquid states and pairing instability of a general model of copper oxide metals, Phys. Rev. B **55**, 14554 (1997).

[36] H. Yokoyama, S. Tamura, and M. Ogata, Staggered flux state in two-dimensional hubbard models, J. Phys. Soc. Jpn. **85**, 124707 (2016).

[37] H. Kontani, Y. Yamakawa, R. Tazai, and S. Onari, Odd-parity spin-loop-current order mediated by transverse spin fluctuations in cuprates and related electron systems, Phys. Rev. Research **3**, 013127 (2021).

[38] S. Bulut, W. A. Atkinson, and A. P. Kampf, Spatially modulated electronic nematicity in the three-band model of cuprate superconductors, Phys. Rev. B **88**, 155132 (2013).

[39] Y. Wang and A. V. Chubukov, Charge-density-wave order with momentum $(2Q, 0)$ and $(0, 2Q)$ within the spin-fermion model: Continuous and discrete symmetry breaking, preemptive composite order, and relation to pseudogap in hole-doped cuprates, Phys. Rev. B **90**, 035149 (2014).

[40] R.-Q. Xing, L. Classen, and A. V. Chubukov, Orbital order in FeSe: The case for vertex renormalization, Phys. Rev. B **98**, 041108(R) (2018).

[41] T. Holder and W. Metzner, Incommensurate nematic fluctuations in two-dimensional metals, Phys. Rev. B **85**, 165130 (2012).

[42] M. A. Metlitski and S. Sachdev, Instabilities near the onset of spin density wave order in metals, New J. Phys. **12**, 105007 (2010); S. Sachdev and R. La Placa, Bond Order in Two-Dimensional Metals with Antiferromagnetic Exchange Interactions, Phys. Rev. Lett. **111**, 027202 (2013).

[43] J. C. S. Davis and D.-H. Lee, Concepts relating magnetic interactions, intertwined electronic orders, and strongly correlated superconductivity, Proc. Natl. Acad. Sci. U.S.A. **110**, 17623 (2013).

[44] E. Berg, E. Fradkin, S. A. Kivelson, and J. M. Tranquada, Striped superconductors: How spin, charge and superconducting orders intertwine in the cuprates, New J. Phys. **11**, 115004 (2009).

[45] Y. Yamakawa, and H. Kontani, Spin-Fluctuation-Driven Nematic Charge-Density Wave in Cuprate Superconductors: Impact of Aslamazov-Larkin Vertex Corrections, Phys. Rev. Lett. **114**, 257001 (2015).

[46] M. Tsuchiizu, Y. Yamakawa, and H. Kontani, p-orbital density wave with d symmetry in high-T_c cuprate superconductors predicted by renormalization-group + constrained RPA theory, Phys. Rev. B **93**, 155148 (2016).

[47] M. Tsuchiizu, K. Kawaguchi, Y. Yamakawa, and H. Kontani, Multistage electronic nematic transitions in cuprate superconductors: A functional-renormalization-group analysis, Phys. Rev. B **97**, 165131 (2018).

[48] K. Kawaguchi, Y. Yamakawa, M. Tsuchiizu, and H. Kontani, Competing unconventional charge-density-wave states in cuprate superconductors: Spin-fluctuation-driven mechanism, J. Phys. Soc. Jpn. **86**, 063707 (2017).

[49] S. Onari and H. Kontani, Self-consistent Vertex Correction Analysis for Iron-based Superconductors: Mechanism of Coulomb Interaction-Driven Orbital Fluctuations, Phys. Rev. Lett. **109**, 137001 (2012).

[50] Y. Yamakawa, S. Onari, and H. Kontani, Nematicity and Magnetism in FeSe and Other Families of Fe-Based Superconductors, Phys. Rev. X **6**, 021032 (2016).

[51] S. Onari, Y. Yamakawa, and H. Kontani, Sign-Reversing Orbital Polarization in the Nematic Phase of FeSe due to the C_2 Symmetry Breaking in the Self-Energy, Phys. Rev. Lett. **116**, 227001 (2016).

[52] S. Onari and H. Kontani, Origin of diverse nematic orders in Fe-based superconductors: 45 degree rotated nematicity in AFe_2As_2 (A=Sc, Rb), Phys. Rev. B **100**, 020507(R) (2019).

[53] S. Onari and H. Kontani, Hidden antiferronematic order in Fe-based superconductor $BaFe_2As_2$ and NaFeAs above T_S, Phys. Rev. Research **2**, 042005(R) (2020).

[54] R. Tazai and H. Kontani, Multipole fluctuation theory for heavy fermion systems: Application to multipole orders in CeB_6, Phys. Rev. B **100**, 241103(R) (2019).

[55] W. Metzner, M. Salmhofer, C. Honerkamp, V. Meden, and K. Schönhammer, Functional renormalization group approach to correlated fermion systems, Rev. Mod. Phys. **84**, 299 (2012).

[56] C. Honerkamp, Charge instabilities at the metamagnetic transition of itinerant electron systems, Phys. Rev. B **72**, 115103 (2005).

[57] C. Husemann and W. Metzner, Incommensurate nematic fluctuations in the two-dimensional Hubbard model, Phys. Rev. B **86**, 085113 (2012).

[58] M. Tsuchiizu, Y. Ohno, S. Onari, and H. Kontani, Orbital Nematic Instability in the Two-Orbital Hubbard Model: Renormalization-Group + Constrained RPA Analysis, Phys. Rev. Lett. **111**, 057003 (2013).

[59] R. Tazai, Y. Yamakawa, M. Tsuchiizu, and H. Kontani, Functional renormalization group study of orbital fluctuation mediated superconductivity: Impact of the electron-boson coupling vertex corrections, Phys. Rev. B **94**, 115155 (2016).

[60] H. Kino and H. Fukuyama, Phase diagram of two-dimensional organic conductors: $(BEDT-TTF)_2X$, and references therein, J. Phys. Soc. Jpn. **65**, 2158 (1996).

[61] B. J. Powell and R. H. McKenzie, Quantum frustration in organic Mott insulators: From spin liquids to unconventional superconductors, Rep. Prog. Phys. **74**, 056501 (2011).

[62] See Supplemental Material at http://link.aps.org/supplemental/10.1103/PhysRevResearch.3.L022014 for additional explanation for RG+cRPA method, and additional numerical results for $t'/t = 0.7$ in κ-$(BEDT-TTF)_2X$ model are presented.

[63] W. Ku, T. Berlijn, and C.-C. Lee, Unfolding First-Principles Band Structures, Phys. Rev. Lett. **104**, 216401 (2010).